Originals Computational Mechanics 20 (1997) 285–294 © Springer-Verlag 1997

Parametrized variational principles in dynamics applied to the optimization of dynamic models of plates

F. J. Brito Castro, C. Militello, C. A. Felippa

Abstract We investigate the use of Parametrized Variational Principles (PVP) in linear structural dynamics. Our main objective is to assess whether the free parameters can be used to enhance the accuracy of dynamic models on a fixed mesh. Consistent, boundary-consistent and lumped mass matrices are defined within the framework of the PVP. The accuracy provided by three different mass matrices in the computation of plate frequencies is numerically studied. A method to update the free parameters on an element by element basis to improve the dynamic model is presented. Numerical experiments that characterize that improvement for the vibration and transient-response analysis of plates are presented. These experiments suggest that such update is primarily beneficial for modes in the intermediate frequency range.

1 Introduction

Parametrized variational principles (PVPs) originally evolved from an effort to provide a variational framework to the finite-element Free Formulation (FF) of Bergan and Mygård (1984) and the Assumed Natural Strain (ANS) formulation of Park and Stanley (1986). This technique has advanced in generality to produce formulations where the variational principles of classical mechanics are particular cases of a multifield functional with free parameters. Two recent review papers, Felippa (1994, 1996) survey the methodology and applications.

For the case of compressive linear elastostatics, Felippa and Militello (1989, 1990) have shown that a general multifield PVP in which displacements are independently varied contains three free parameters in the internal energy. This form contains the well known principles of Total Potential Energy, Hellinger-Reissner and Hu-Washizu as particular cases. The principle of Total Complementary Energy can be embedded in a one-parameter form without independently varied displacements.

Finite elements for structural and solid mechanics based on PVPs will naturally retain any free parameter kept in the generating functional. These are called "parametrized elements." An important question is: can the selection of free parameters affect convergence? If one accepts the view that passing the Patch Test, in conjunction with stability conditions (rank sufficiency), fulfills the convergence requirement, the answer is negative. Militello and Felippa (1991a) have shown that the application of the Individual Element Test (IET) originally proposed by Bergan and Hanssen (1974) guarantees that forms A, B and C of the Patch Test described by Taylor et al. (1986) are satisfied. Because the free parameters have no effect on the IET as long as rank sufficiency is preserved, it follows that selection of the free parameters will primarily affect the *accuracy* performance of parametrized elements.

Moreover, we can use a different set of free parameters for different elements (and thus effectively a different variational principle for each element), without affecting the convergence criteria set by the Patch Test. Up to now the free parameters have been chosen in order to obtain maximum accuracy for coarse meshes in static problems. In this paper we seek to establish the necessary basis to select parameters in order to optimize the linear dynamic response of structures modeled with parametrized elements. The numerical studies have focused on plate elements.

2 Parametrized variational principles

Consider a linear hyperelastic body of volume V. To use hybrid functionals the body is divided into subdomains, which in the FEM treatment become individual elements. The boundary S consists of three parts: S_t, S_u and S_i. S_t is the portion of S over which surface tractions $\hat{\mathbf{t}}$ are specified; S_u is the portion over which displacements $\hat{\mathbf{u}}$ are specified, and S_i is the union of internal interfaces when the body is divided into finite elements. The body force field $\mathbf{b}$ is given inside V.

A hybrid PVP is constructed from two basic ingredients: the parametrized internal energy functional U and a potential P^d that includes the contribution of the internal interfaces:

$$\Pi^d(\tilde{\mathbf{u}}, \tilde{\boldsymbol{\sigma}}, \tilde{\mathbf{e}}, \tilde{\mathbf{d}}) = U(\tilde{\mathbf{u}}, \tilde{\boldsymbol{\sigma}}, \tilde{\mathbf{e}}, \tilde{\mathbf{d}}) - P^d(\tilde{\mathbf{u}}, \tilde{\boldsymbol{\sigma}}, \tilde{\mathbf{e}}, \tilde{\mathbf{d}}) \qquad (1)$$

where

Communicated by I. Singh, 16 January 1997

F. J. Brito Castro, C. Militello
Departamento de Física Fundamental y Experimental, Universidad de La Laguna, Av. Astrofísico Francisco Sánchez s/n, La Laguna, Tenerife 38203, Spain

C. A. Felippa
Department of Aerospace Engineering Sciences, and Center for Aerospace Structures, University of Colorado at Boulder, Boulder, CO 80309-0429, USA

Correspondence to: C. A. Felippa

$$P^d(\tilde{\mathbf{u}},\tilde{\boldsymbol{\sigma}},\tilde{\mathbf{e}},\tilde{\mathbf{d}}) = \int_V \mathbf{b}\tilde{\mathbf{u}}\,\mathrm{d}V + \int_{S_t} \hat{\mathbf{t}}\tilde{\mathbf{d}}\,\mathrm{d}S + \int_S \tilde{\sigma}_n(\tilde{\mathbf{u}}-\tilde{\mathbf{d}})\,\mathrm{d}S \tag{2}$$

$$U(\tilde{\mathbf{u}},\tilde{\boldsymbol{\sigma}},\tilde{\mathbf{e}},\tilde{\mathbf{d}}) = \frac{1}{2}\int_V \begin{Bmatrix} \tilde{\boldsymbol{\sigma}} \\ \boldsymbol{\sigma}^e \\ \boldsymbol{\sigma}^u \end{Bmatrix}^T \begin{bmatrix} j_{11} & j_{12} & j_{13} \\ j_{21} & j_{22} & j_{23} \\ j_{31} & j_{32} & j_{33} \end{bmatrix} \begin{Bmatrix} \tilde{\boldsymbol{\sigma}} \\ \boldsymbol{\sigma}^e \\ \boldsymbol{\sigma}^u \end{Bmatrix} \mathrm{d}V \tag{3}$$

Here superscripts indicates a dependent field and the superposed tilde indicates an independently, primary, varied field. Expression (2) assumes that the varied displacements satisfy strongly the prescribed-displacement B.C. on S_u; otherwise an additional integral appears.

Three independently varied fields: displacements $\tilde{\mathbf{u}}$, $\tilde{\boldsymbol{\sigma}}$ and strains $\tilde{\mathbf{e}}$ are defined inside each element, and need not be conforming across elements boundaries. The connection between elements is effected through an independently varied displacement field $\tilde{\mathbf{d}}$, which is only defined at element boundaries. In (2) $\boldsymbol{\sigma}_n$ is the projection of $\tilde{\boldsymbol{\sigma}}$ on the boundary normal n. The free parameters in (3) are denoted by j_{ik}.

The boundary displacement $\tilde{\mathbf{d}}$ must be uniquely defined over each element side by nodal values $\mathbf{v}$ taken over that side. Boundary conformity with adjacent elements is thereby guaranteed. These nodal values are the only unknowns that survive static condensation at the element level. Before condensation takes place, relationships between the internal independent fields and the field may be enforced to simplify U. In order to preserve the variational character of the formulation those relationships are weakly imposed through Lagrange-multipliers. Consistency of the Euler equations reduce the nine independent parameters to three. Technical details for these manipulations are provided by Felippa and Militello (1989, 1990).

If we choose the three diagonal entries j_{ii} as the independent ones, we obtain the representation depicted in Fig. 1. Here j_{11}, j_{22} and j_{33} are used as axes in a three-dimensional plot that marks important elasticity functionals. In this figure HW, HR and PE stand for Hu-Washizu, Hellinger-Reissner and the Potential Energy variational principles, respectively.

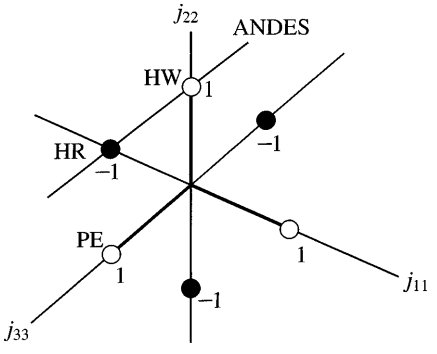

Fig. 1. The space of functionals spanned by the PVP (1)–(3)

3
The stiffness equations

For FEM discretization, the internal independent fields of the multifield PVP are split into a part associated with rigid body motions and constant strain states, and a part associated with higher order strains, as schematically shown in Fig. 2. Generalizing previous results of Bergan and Nygård (1984), Militello (1991) showed that orthogonality constraints between the basic and higher order parts results from the imposition of the IET, for any selection of free parameters.

The element-level static condensation process outlined above provides the element stiffness equations

$$\mathbf{K}\mathbf{v} = (\mathbf{K}_b + \mathbf{K}_h)\mathbf{v} = \mathbf{f} \tag{4}$$

where

- $\mathbf{v}$ the nodal degrees of freedom that define $\tilde{\mathbf{d}}$ over the element boundary
- $\mathbf{f}$ the nodal force vector consistent with $\mathbf{b}$ and $\hat{\mathbf{t}}$ (this vector is independent of the free parameters)
- $\mathbf{K}_b$ the basic stiffness matrix, which is associated with the rigid body modes and constant strain states, and
- $\mathbf{K}_h$ the higher order stiffness matrix, which is associated with the higher order strain states.

3.1
Dependence of stiffness on free parameters

All finite elements used in the present research derive from the PVP in which the stress field $\tilde{\boldsymbol{\sigma}}$ is assumed *constant* inside the element (cf. Fig. 2) and thus affects only the basic stiffness matrix $\mathbf{K}_b$. Therefore, the higher order stiffness depends only on the assumed internal displacements field $\tilde{\mathbf{u}}$ and strain field $\tilde{\mathbf{e}}$. The structure of $\mathbf{K}_h$ as a function of these two fields and of the independent free parameters j_{ii} is as a function of the proposed independent fields and the independent parameters is the following:

$$\mathbf{K}_h = \tfrac{1}{2}\mathbf{K}_h^{u,e} + \tfrac{1}{2}j_{11}\mathbf{K}_h^{u,e} + j_{22}(\mathbf{K}_h^e - \tfrac{1}{2}\mathbf{K}_h^{u,e}) + j_{33}(\mathbf{K}_h^u - \tfrac{1}{2}\mathbf{K}_h^{u,e}) \tag{5}$$

where

$$\mathbf{K}_h^u = \int_V (\mathbf{B}_h^u)^T\mathbf{E}\mathbf{B}_h^u\,\mathrm{d}V, \qquad \mathbf{K}_h^e = \int_V (\mathbf{B}_h^e)^T\mathbf{E}\mathbf{B}_h^e\,\mathrm{d}V\ ,$$
$$\mathbf{K}_h^{u,e} = \int_V \left((\mathbf{B}_h^u)^T\mathbf{E}\mathbf{B}_h^e + (\mathbf{B}_h^e)^T\mathbf{E}\mathbf{B}_h^u\right)\mathrm{d}V\ . \tag{6}$$

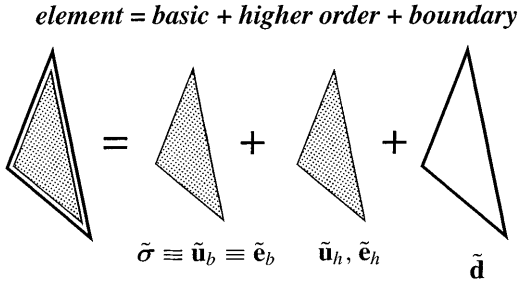

Fig. 2. Field assumptions used in the construction of hybrid PVP elements

Here $\mathbf{E}$ is the matrix of stress-strain coefficients, and the $\mathbf{B}_h^x$ are strain-displacement matrices that relate higher order strains to the element degrees of freedom $\mathbf{v}$. The superscript of that matrix indicates the independent field from which it is derived.

Matching (5) with Fig. 1 one can see how the element stiffness, the variational principles and the values of the free parameters j_{ii} are related.

If we choose $j_{22} = j_{11} + 1$ and $j_{33} = 0$ the contribution of the internal displacement field $\tilde{\mathbf{u}}$ to the higher order strains vanishes. This is the case for the ANDES (Assumed Natural DEviatoric Strains) formulation for which

$$\mathbf{K}_h = (j_{11} + 1)\mathbf{K}_h^e = \alpha \mathbf{K}_h^e \tag{7}$$

Here $\alpha = j_{11} + 1$ may be taken to be the free parameter for notational convenience, as in the original development by Militello and Felippa (1991). Note that if $j_{11} = -1, \alpha = 0$; in which case the element stiffness matrix $\mathbf{K}$ reduces to the basic stiffness $\mathbf{K}_b$, which is in general rank deficient.

4
Mass matrices

Another key ingredient in linear dynamic analysis of undamped structures is the mass matrix $\mathbf{M}$, which results from the discretization of the kinetic energy.

The formulation of this matrix within the PVP framework has not been systematically explored. The kinetic energy is a function of the velocity field, which derives directly from the element displacement field. But in hybrid PVP elements there are two kinds of displacements. This dichotomy is expressed by two interpolation formulas, one for the interior and one for the boundary:

$$\tilde{\mathbf{u}} = \mathbf{N}_u \mathbf{q}, \qquad \tilde{\mathbf{d}} = \mathbf{N}_d \mathbf{v} \tag{8}$$

Here $\mathbf{N}_u$ collects interpolation functions in terms of the generalized coordinates $\mathbf{q}$, whereas $\mathbf{N}_d$ collects boundary shape functions in terms of the element degrees of freedom $\mathbf{v}$. Note that the second of (8) is only defined at element boundaries.

Following the Free Formulation (FF) approach, the interior displacement $\tilde{\mathbf{u}}$ is separated into the contribution to the basic (rigid body modes and constant strain states) and higher order parts:

$$\tilde{\mathbf{u}} = \mathbf{N}_{rc}\mathbf{q}_{rc} + \mathbf{N}_h \mathbf{q}_h \tag{9}$$

As in the FF, we now impose that the number of parameters $\mathbf{q}$ and number of degrees of freedom in $\mathbf{v}$ be the same. Collocating the value of $\tilde{\mathbf{u}}$ at the element nodes we obtain

$$\tilde{\mathbf{u}} = \mathbf{G}_{rc}\mathbf{q}_{rc} + \mathbf{G}_h \mathbf{q}_h = \mathbf{G}\mathbf{q} \tag{10}$$

where $\mathbf{G}$ is a square matrix, which is assumed to be nonsingular. Its inverse is called $\mathbf{H} = \mathbf{G}^{-1}$. This matrix can be partitioned as

$$\mathbf{q} = \mathbf{H}\mathbf{v} = \begin{bmatrix} \mathbf{H}_{rc} \\ \mathbf{H}_h \end{bmatrix} \mathbf{v} \tag{11}$$

4.1
Consistent mass matrix

Applying D'Alembert's principle we replace in (2) the body forces $\mathbf{b}$ by $-\rho\ddot{\mathbf{u}}$. The constraints connecting the internal fields and the boundary displacement $\tilde{\mathbf{d}}$ must hold for each time t. This can still be satisfied with Lagrange multipliers because the constraints are holonomic. The specified boundary tractions are assumed to be conservative.

To obtain a dynamic PVP, the integrations in (2) are extended to include the time domain. Upon integrating by parts one obtains a parametrized form of Hamilton's principle, in which the free parameters affect only the potential energy. Upon taking variations, replacing the continuous fields by discrete ones and performing the static condensation process, we recover as Euler equations the discrete equations of motion

$$\mathbf{M}\ddot{\mathbf{v}} + \mathbf{K}\mathbf{v} = \mathbf{f} \tag{12}$$

where $\mathbf{f} = \mathbf{f}(t)$ and $\mathbf{v} = \mathbf{v}(t)$ represents the dynamic nodal forces and nodal displacement response, respectively. The stiffness matrix coincides with that derived in Sect. 3.1, while the mass matrix is

$$\mathbf{M} = \mathbf{H}^T \left(\int_V \begin{bmatrix} \mathbf{N}_{rc}\mathbf{N}_{rc} & \mathbf{N}_{rc}\mathbf{N}_h^T \\ \mathbf{N}_h\mathbf{N}_{rc}^T & \mathbf{N}_h\mathbf{N}_h^T \end{bmatrix} \mathrm{d}V \right) \mathbf{H} \tag{13}$$

This matrix will be called a *consistent mass matrix* or CMM in the present approach. Some similarities and differences with the consistent mass matrices of standard FEM should be noted.

(a) The mass matrix (13) is constructed from an interior displacement field $\tilde{\mathbf{u}}$ defined within the element. This field does not necessarily equals $\tilde{\mathbf{d}}$ at all boundary points, since we have enforced the matching (10) only at the nodes.
(b) The expression (13) is variationally consistent regardless of whether the interior displacement $\tilde{\mathbf{u}}$, or part thereof, is used to compute the element stiffness $\mathbf{K}$.
(c) The mass matrix (13) does not contain information about the boundary displacement $\tilde{\mathbf{d}}$.
(d) For displacement-conforming finite elements, (13) reduces to the conventional CMM, since in that case the boundary and interior displacement fields match.

Point (b) needs further explanation. Let us assume that we specialize the general 3-parameter PVP (3) by taking $j_{22} = j_{11} + 1$, $j_{33} = 0$, which is the case for the ANDES formulation. If so the assumed higher order strains are not necessarily compatible, that is, derivable point by point from a displacement field. Nevertheless the mass matrix (13) will still be variationally consistent with that formulation.

4.2
Boundary-consistent and lumped mass matrices

The name *boundary-consistent mass matrix* or BCMM identifies here a mass matrix obtained from the boundary displacement field only. Imagine a process that lumps the mass of the element over the element boundary. For a three-dimensional (3D) element this process produces a mass $\bar{m}$ per unit of boundary area. On the other hand, for the 2D case, such as the plate elements considered in subsequent Sections, this process produces a mass $\bar{m}$ per unit of boundary length.

The contribution of this boundary mass to the element degrees of freedom is consistently obtained using the boundary displacement $\tilde{\mathbf{d}} = \mathbf{N}_d\mathbf{v}$. In the 3D case this is defined by a surface integral:

$$\int_{S_e} \bar{m}\mathbf{N}_d\mathbf{N}_t \, dS \tag{14}$$

where S_e is the element boundary. The equivalent formula for 2D elements involves a line-contour integral.

The main advantage of the BCMM is that we only need to know the boundary displacement whereas the interior displacement field is not required. This eliminates the complex calculations required in (9), (10), (11) and (13). As an example, for a three node Kirchhoff (C^1) plate element with 9 degrees of freedom, the BCMM may be obtained simply through the assembly of the consistent mass of three Hermitian beams placed along the element boundary. Similarly if the plate element is of Reissner-Mindlin (C^0) type, the consistent mass matrix of three Timoshenko boundary beams would be assembled.

Finally the *lumped mass matrix* or LMM is obtained by a procedure that directly distributes the element mass to the nodes, resulting in a diagonal **M**. This can be done in several ways. In the 3-node triangular element for a Kirchhoff plate, a straightforward approach would be to assemble the well known lumped mass matrices of the variable-area Hermitian beams. Alternatively diagonalization of the BCMM matrix can be effected by a variety of techniques surveyed, for instance in Cook, Malkus and Plesha (1992).

4.3
A plate-frequency convergence study

Here we study the convergence rate of the AQR-ANDES Kirchhoff triangular plate element, developed by Militello and Felippa (1991b), for a simple free-vibrations problem. This element has three corner nodes and 9 degrees of freedom. We discretize a square plate simply supported at its four boundaries (SS1 condition). For the convergence studies we start from the mesh shown in Fig. 3. Each new refined mesh is obtained from the previous one following the nested triangle splitting indicated by the dashed lines.

We compute the eigenvectors and eigenvalues using the same free parameter, $\alpha = 1$ for each triangle in the mesh. Three mass matrices of type CMM, BCMM and LMM, respectively, are used.

The consistent mass matrix (CMM) is constructed using the transverse displacement field $w = w_b + w_h$ proposed by Felippa and Bergan (1987) for a bending triangle based on the Free Formulation. Denoting as usual the triangular coordinates by ζ_1, ζ_2 and ζ_3, the transverse displacement field associated with the rigid body motions and constant strains is represented by

$$\begin{aligned} w_b = {} & (1 + \zeta_1 - \zeta_2)q_1 + (1 + \zeta_2 - \zeta_3)q_2 \\ & + (1 + \zeta_3 - \zeta_1)q_3 + (\zeta_1 - \zeta_2)^2 q_4 \\ & + (\zeta_2 - \zeta_3)^2 q_5 + (\zeta_3 - \zeta_1)^2 q_6 \end{aligned} \tag{15}$$

whereas the energy-orthogonal displacement associated with the higher order deformations (in this case, linearly-varying plate curvatures) is

$$w_h = (\zeta_1 - \zeta_2)^3 q_7 + (\zeta_2 - \zeta_3)^3 q_8 + (\zeta_3 - \zeta_1)^3 q_9 \tag{16}$$

Felippa and Bergan (1987) show that this choice leads to a nonsingular matrix **G** in (10), which moreover has an inverse **H** computable in closed form.

The BCMM is obtained by assembling the mass matrix of three Hermitian side beams constructed as described in Militello and Felippa (1991a). The LMM is a row-sum diagonalization of the BCMM.

The log-log plots in Figs. 4 and 5 show the convergence rate of the computed frequencies for vibration modes $n = 4$ and $n = 7$, respectively. The error is reported as $\ln|(\omega_i^{\text{FEM}}/\omega_i) - 1|$, where ω_i is the exact frequency for the i^{th} vibration mode. The abscissa is the length of an element

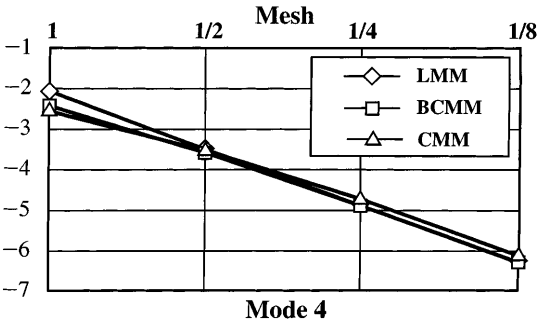

Fig. 4. Convergence of mode 4 for SS square plate using three mass matrices meshes 1 through 4

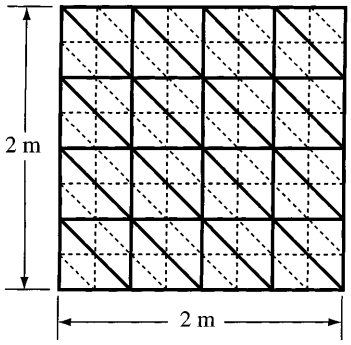

MESH	ELEMENTS
1	32
2	128
3	512
4	2048
5	8192

$E = 200 \times 10^9$ Pa
$\rho = 7800$ kg/m^3
$\nu = 0.28$
$h = 0.01$ m

Fig. 3. Simply supported (SS) square plate. Basic FE mesh and physical properties

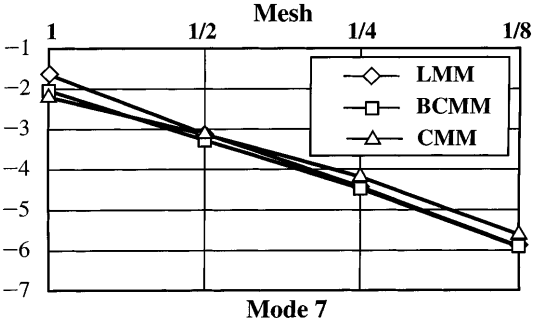

Fig. 5. Convergence of mode 7 for SS square plate using three mass matrices and meshes 1 through 4

side normalized with respect to that in the basic 4×4 mesh. Convergence behavior for other natural frequencies displays a similar behavior. As can be seen, the convergence rate is similar for the three matrices. This example suggests that the additional complexity required by the construction of a CMM cannot be justified on the grounds of eigenvalue accuracy, as is the case for conforming finite elements.

Further physical insight into the nature of the discretization error can be gained from studying the Rayleigh-quotient (RQ) approximation of the vibration eigenvalues (the squared frequencies). Denoting by $\mathbf{x}_a$ a eigenvector approximation to the i^{th} mode, we decompose the associated RQ as follows

$$R = \frac{\mathbf{x}_a^T \mathbf{K} \mathbf{x}_a}{\mathbf{x}_a^T \mathbf{M} \mathbf{x}_a} = \frac{\mathbf{x}_a^T \mathbf{K}_b \mathbf{x}_a}{\mathbf{x}_a^T \mathbf{M} \mathbf{x}_a} + \frac{\mathbf{x}_a^T \mathbf{K}_h \mathbf{x}_a}{\mathbf{x}_a^T \mathbf{M} \mathbf{x}_a} = R_b + R_h \tag{17}$$

R_b and R_h identify the contributions of the basic and higher order elastic energies, respectively, to the squared frequency.

Figure 6 shows the evolution of the error $(\omega_i^2 - R)/\omega_i^2$ expressed in %, for modes $i = 1, 4$ and 7 in the plate problem. Figure 7 shows the ratio R_h/R_b for the same eigenvalues.

We can observe a similar trend between convergence and energy ratios. For example, if one looks at the 3% RQ error range, the higher order energy is seen to be just 6% of the total. Thus, the ratios R_h/R_b or R_h/R can be viewed as an indicator of how well we have captured an eigenpair. Furthermore, since free parameters only affect the higher order stiffness, once a specific eigenpair is captured variations of the free parameter will have only a second order effect on frequency accuracy.

With this information in mind, we now investigate the following question: can the free parameters be used to improve the accuracy of higher order vibration modes on a given mesh? In other words, if the dynamic model is fixed (as is often the case in engineering practice) can additional accuracy be "squeezed" by adjusting the higher order stiffness? This is investigated in the following Section using the vibration and transient response of plates as focus problem.

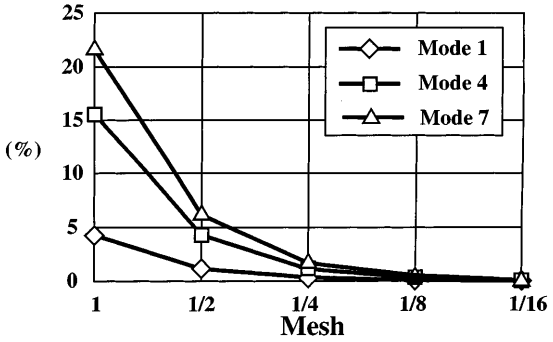

Fig. 6. Evolution of RQ-estimated error $(\omega_i^2 - R)/\omega_i^2$ for modes 1, 4 and 7 of SS square plate using meshes 1 through 5

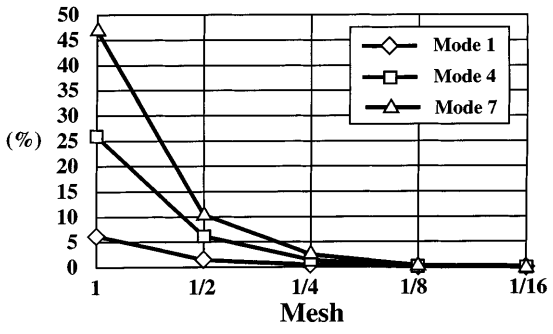

Fig. 7. Evolution of R_h/R_b for modes 1, 4 and 7 of SS square plate using meshes 1 through 5

5
Updating the free parameters

In this section we consider a FEM assembly of N^e parametrized elements forming a dynamic model. Superscript e is used to identify individual elements.

5.1
Objective function

Computed eigenvalues and eigenvectors of the free-vibrations eigenproblem satisfy the following matrix equation at the assembly level:

$$\sum_e (\mathbf{K}^e - \omega_i^2 \mathbf{M}^e) \mathbf{x}_i^e = \mathbf{0} \tag{18}$$

This dynamic equilibrium condition is not satisfied at the element level:

$$\mathbf{r}_i^e = (\mathbf{K}^e - \omega_i^2 \mathbf{M}^e) \mathbf{x}_i^e \neq \mathbf{0} \tag{19}$$

From (18) it follows that the assembly of dynamic force residuals cancels:

$$\sum_e \mathbf{r}_i^e = \mathbf{0} \tag{20}$$

In the present work we consider only ANDES elements characterized by the one-parameter higher order stiffness representation (7), which at the element level is written

$$\mathbf{K}^e = \mathbf{K}_b^e + \alpha^e \mathbf{K}_b^e \tag{21}$$

where α^e are the N_e free parameters at our disposal to improve the quality of the dynamic model. There is one parameter per element. Introducing this into (19) yields

$$\mathbf{r}_i^e = \mathbf{K}_b^e \mathbf{x}_i^e + \alpha^e \mathbf{K}_h^e - \omega_i^2 \mathbf{M}^e \mathbf{x}_i^e \tag{22}$$

From (22) the following term is extracted:

$$\mathbf{R}_i^e = \alpha^e \mathbf{K}_h^e - \omega_i^2 \mathbf{M}^e \mathbf{x}_i^e \tag{23}$$

For each i^{th} eigenpair, the assembly of (23) no longer results in a null vector,

$$\mathbf{R}_i = \sum_e \mathbf{R}_i^e \neq \mathbf{0} \tag{24}$$

As objective function to be minimized with respect to the α^e in order to improve the approximation, we propose to use the Euclidean norm of (24). The problem is complicated, however, by the fact that if we consider a set of $i = 1, \ldots, M$ modes as participating in the dynamic response, we have M vectors (24) that can be arranged in a supervector

$$\mathbf{R}_{1,M}^T = [\mathbf{R}_1^T \quad \mathbf{R}_2^T \ \ldots \ \mathbf{R}_M^T] \tag{25}$$

In this case the objective function is taken to be the Euclidean norm of (25). If the residual vector, however, contains components of different physical dimensions (for example, forces and moments in the case of the plate problem), it is necessary to use a weighted norm that scales the components to have the same physical dimension. Use of that kind of scaling is tacitly assumed in the sequel.

5.2
Parameter update

We now describe the procedure to update the parameters α^e in order to minimize the objective function. The procedure is described first in terms of fitting one eigenpair $(\omega_i, \mathbf{x}_i)$ indexed by i, and then generalized to a eigenpair range.

The procedure is a simplified form of the sensitivity-based, element-by-element (SB-EBE) updating procedure developed by Hemez (1993); see also Farhat and Hemez (1993). The update procedure does not necessarily includes all of the elements and mesh degrees of freedom. To decide whose elements will be subjected to update for a given eigenpair index i, the following element-level error indicator is used:

$$\epsilon_i^e = \frac{\|\mathbf{L}^e\mathbf{R}_i\|_2}{\|\mathbf{R}_i\|_2} = \frac{\|\mathbf{P}^e\|_2}{\|\mathbf{R}_i\|_2} \tag{26}$$

where $\mathbf{L}^e$ is the localization matrix that isolates the components of vector $\mathbf{R}_i$ associated with the degrees of freedom of element e. Vector $\mathbf{P}^e$ is a patch dynamic residual. It should be noticed that $\mathbf{P}^e = \mathbf{L}^e\mathbf{R}_i \neq \mathbf{R}_i^e$ because $\mathbf{P}^e$ includes the contribution from neighboring elements to the selected degrees of freedom. If ϵ_i^e, evaluated initially with all α^e set to unity, is less than a threshold, element e is dropped. The degrees of freedoms connected to the retained elements define the freedom subset that participates in the update stage described next.

The procedure starts by setting $\alpha^e = 1$ for all elements. This initial model is identified as the Non-Updated configuration or NU. Assume that after the last update step the parameters are α^e. The increments to be determined in the next step are $\Delta\alpha^e$, where e ranges over the retained elements for mode index i.

We look for a minimum of the quadratic functional:

$$J(\Delta\alpha) = \sum_{i=1}^{M} J_i, \qquad J_i = \left\| \mathbf{R}_i + \left(\sum_e \Delta\alpha_i^e \mathbf{K}_h^e \right) \mathbf{x}_i \right\|_2^2, \tag{27}$$

where M is the number of eigenpairs we seek to improve. The objective function (27) is based on the idea that, away from convergence, the higher order stiffness expands a function basis capable of absorbing the kinetic energy accumulated in the mass matrix.

Imposing that the first variation of the functional (27) equals zero we obtain the following least-squares linear system for each eigenpair:

$$\mathbf{A}_i^T\mathbf{A}_i\delta\alpha = -\mathbf{A}_i\mathbf{R}_i \tag{28}$$

where as noted $\Delta\alpha$ collects the α^e of the N^e elements selected in the update, and $\mathbf{A}_i$ are matrices that emerge from setting $\partial J_i/\partial(\Delta\alpha) = 0$. The number of columns of $\mathbf{A}_i$ is the number N^e os retained elements and the number of rows the number of degrees of freedom connected to those elements.

If we consider all the eigenpairs 1 through M, the minimization results in the following least square algebraic system:

$$\mathbf{A}_B^T\mathbf{A}_G\,\Delta\alpha = -\mathbf{A}^T\mathbf{R}_{1,M} \tag{29}$$

where

$$\mathbf{A}_G^T = [\mathbf{A}_1^T \quad \mathbf{A}_2^T \ \ldots \ \mathbf{A}_M^T] \tag{30}$$

The least squares system (30) is generally singular (or highly ill conditioned) and is solved through a singular value decomposition (SVD). Once the SVD solution is obtained, the parameters are updated:

$$\alpha \to \alpha + \Delta\alpha \tag{31}$$

and a new set of eigenpairs $(\omega_i, \mathbf{x}_i), i = 1, \ldots, M$ is computed. The process is normally carried out for only one iteration.

5.3
Remarks on the choice of objective function

We have proposed the minimization of (27) as a way to update the parameters α^e to obtain improved eigenpairs on a fixed mesh. To numerically assess whether such improvement has occurred, in the present study the new eigenvalues are compared with those computed using a finer mesh. The error indicator attempts to fulfill two objectives:

(a) The parameters obtained by minimizing (27) should provide a new stiffness matrix from which better eigenvalues can be computed.
(b) The new eigenvalues and eigenvectors will produce a smaller value for the norm of $\sum_e \mathbf{R}_i^e$.

At the time of writing we have not investigated the mathematical proof of both properties. Nonetheless, (a) and (b) have been verified in all numerical experiments carried out until now. From that set we extract two examples presented in the next section.

6
Numerical examples

The two examples presented below involve analysis of Kirchhoff plates using the AQR-ANDES triangular element. To measure errors in eigenvalues obtained after we update the parameters, we compare the results computed from a coarse mesh with the ones from a refined mesh. The refined mesh is obtained by nested splitting of each triangle into four. A lumped mass matrix is used throughout.

The results from the initial non-updated coarse mesh and the updated one are identified by NU and U respectively. For the non-updated and refined meshes the free parameters α^e are set to one.

To assess the improvement in the dynamic response we use the following error measures:

$$\epsilon_{\max} = \|f(k) - f^*(k)\|_{\max},\ \epsilon_{\text{rms}} = \frac{\Delta t}{T}\sqrt{\sum_e (f(k) - f^*(k))^2} \tag{32}$$

where T is the total time consider in the response analysis, Δt the time step, $f(k)$ is a response quantity computed with the coarse mesh at a given location at the k^{th} time station, and $f^*(k)$ is the corresponding value computed from a refined mesh.

6.1 Simply supported square plate

The values of the adapted parameters are shown in Fig. 8. The first 9 eigenpairs were used in the updating process. Figure 9 shows the improvement obtained in the frequencies. The value of the ninth frequency in the refined mesh is 99.1 Hz.

To see the effect of the improvement in the dynamic response of the plate we apply a force $F(t)$ at point E. We compute the response at point R using a Wilson-θ integration scheme. The applied force is a superposition of two harmonics:

$$F(t) = 100\sin[2\pi(12.5)t] + 50\sin[2\pi(25)t] \tag{33}$$

and the time step is $\Delta t = 0.0005$ sec.

The acceleration computed for the first 500 integration steps are represented against that obtained for the refined mesh. Figure 10 shows the results for the coarse, non-updated mesh and Fig. 11 for the updated one. Table 1 lists improvements in the values of $\epsilon_{\max}$ and ϵ_{rms} for displacements, velocities and accelerations.

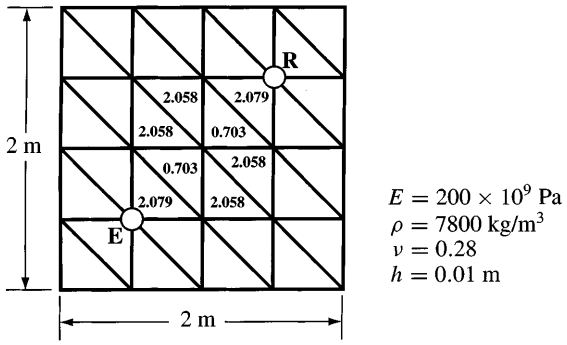

Fig. 8. Basic mesh for dynamic analysis of SS square plate. Updated α^es of 8 retained elements are shown. In transient analysis, force is applied at E and response reported at R

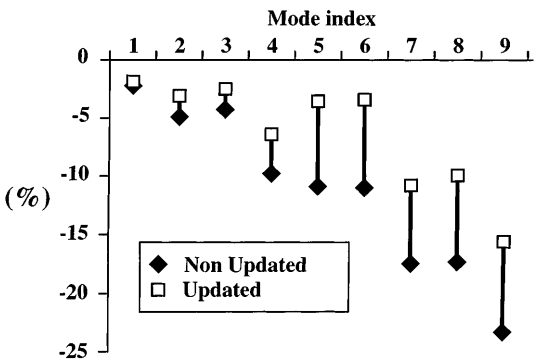

Fig. 9. SS square plate. Frequency errors before and after update procedure on basic mesh

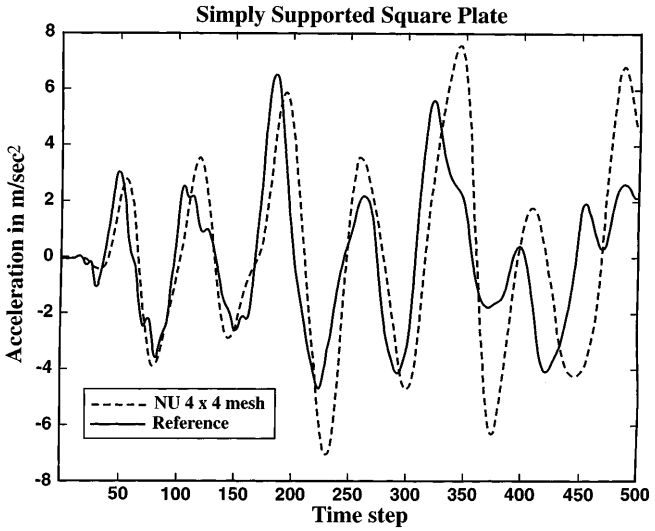

Fig. 10. SS square plate. Acceleration response at point R. Solid line: reference response from fine mesh. Dashed line: response of non-updated basic 4×4 mesh

6.2 Cantilever trapezoidal plate

In Fig. 12 and 13 we can see the new values obtained for the free parameters and the improvement in frequencies.

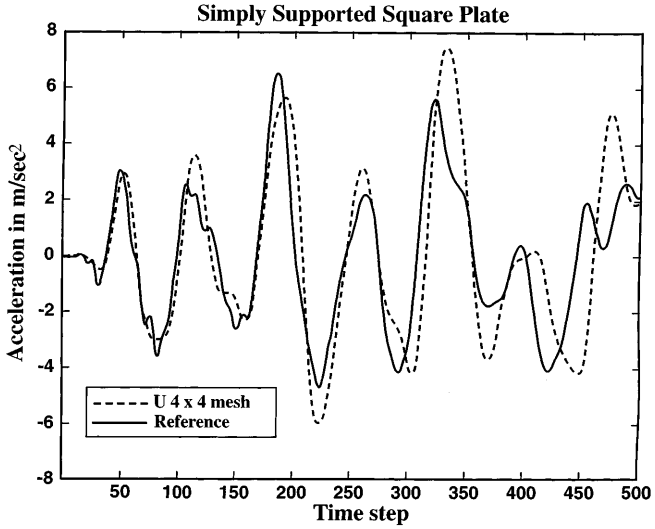

Fig. 11. SS square plate. Acceleration response at point R. Solid line: reference response from fine mesh. Dashed line: response of updated basic 4×4 mesh

Table 1. Improvements in response accuracy for SS square plate

	Displacements		Velocities		Accelerations	
	FEM NU	FEM U	FEM NU	FEM U	FEM NU	FEM U
$\epsilon_{\max}$	186.48	122.92	31.07	26.44	580.95	560.34
ϵ_{rms}	83.43	55.47	13.05	9.03	250.37	184.64

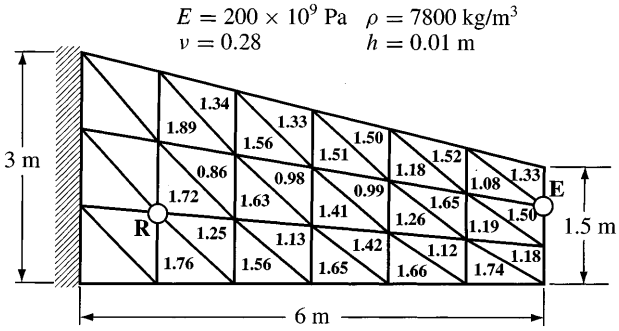

Fig. 12. Cantilever trapezoidal plate. Basic mesh and material properties. Updated α^es of 30 retained elements are shown. In transient analysis, force is applied at E and response reported at R

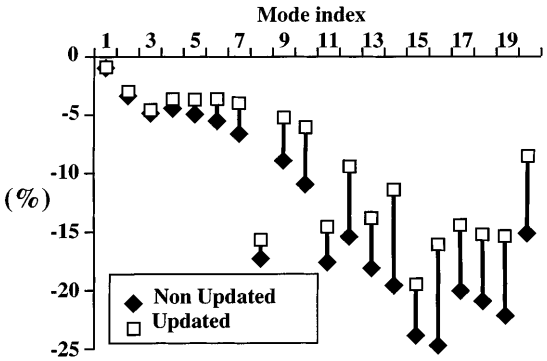

Fig. 13. Cantilever trapezoidal plate. Frequency errors before and after the updating procedure on basic mesh

As predicted before (Sect. 3.1) the update process leaves unchanged the low frequencies. For the update process the first twenty modes were used. Mode 20 in the refined mesh is associated with a frequency of 58.9 Hz.

For this problem the load applied at E is

$$F(t) = 250\sin[2\pi(12.5)t] + 125\sin\left[2\pi(25)t + \frac{\pi}{4}\right] \quad (34)$$

and the time step is again $\Delta t = 0.0005$ sec.

Results were computed for 750 steps, with a total elapsed time of 0.375 seg. Figure 14 shows accelerations computed at point R for the coarse non-updated mesh against the refined one. Figure 15 shows the computed accelerations for the updated mesh. Table 2 lists improvements in the values of $\epsilon_{\max}$ and ϵ_{rms} for displacements, velocities and accelerations.

6.3 Updating mode subsets

As stated before, converged eigenpairs remain largely untouched by parameter updating. These will be collectively called the *low frequency spectrum*, which is accurately captured by the discrete model. The eigenpairs that are reasonably well represented by the model but are sensitive to the parameter choice populate the *intermediate frequency spectrum*. The remaining eigenpairs are strongly mesh dependent and have no physical meaning; they form the *high frequency spectrum*. In structural dynamic problems (as opposed to wave propagation problems) only the modes form the first two subsets are of interest as regards contribution to the response.

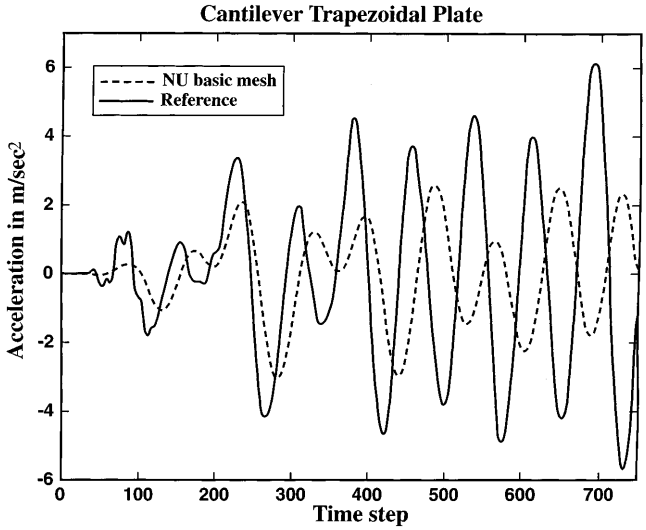

Fig. 14. Cantilever trapezoidal plate. Acceleration at point R. Solid line: reference response from fine mesh. Dashed line: response of non-updated basic mesh

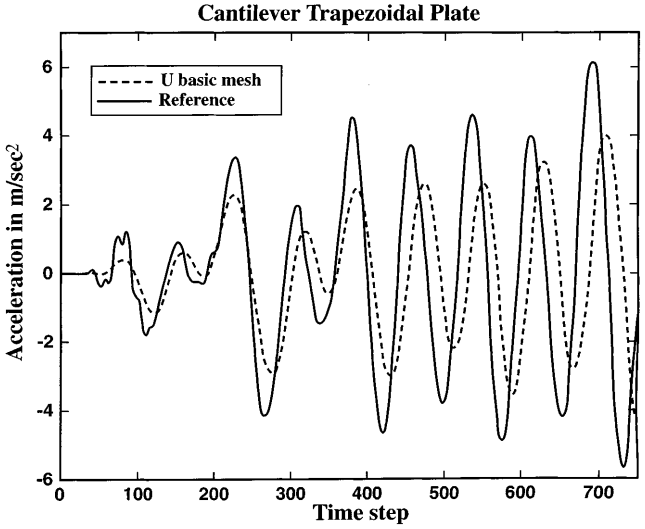

Fig. 15. Cantilever trapezoidal plate. Acceleration at point R. Solid line: reference response from fine mesh. Dashed line: response of updated basic mesh

Table 2. Improvements in response accuracy for cantilever trapezoidal plate

	Displacements		Velocities		Accelerations	
	FEM NU	FEM U	FEM NU	FEM U	FEM NU	FEM U
$\epsilon_{\max}$	341.48	274.92	53.33	42.14	787.94	597.43
ϵ_{rms}	137.09	98.30	20.28	15.22	317.90	236.17

Note that as the finite element model is refined, the separation between these sets change. In regular meshes of simple geometries eigenpairs in the three sets are generally well ordered by frequency value, but in complex, graded

models with diverse structural components, overlapping may occur.

Two intriguing questions that bear on this kind of dynamic modeling are:

(i) How can an eigenpair be categorized into one of the three subsets?
(ii) Can the parameter updating scheme be circumscribed to the subset of intermediate frequency modes without significant degradation in accuracy?

To investigate the answer to (ii) we carried out the parameter update process for the two previous examples but retaining the last 5 and 10 modes, respectively, as update drivers. Tables 3 and 4 show the parameters computed using these reduced sets of eigenpairs and the previous ones. Only small changes are noticeable.

We have also computed the two-norm of vector $\mathbf{R}_{1,M}$ with the old and the new eigenpairs for each case. The results are shown in Tables 5 and 6. The values obtained are revealing. After the update procedure the new stiffness matrix and eigenpairs reduce the two-norm of that vector. However, lower eigenpairs contribute very little to the norm of this vector. For the trapezoidal cantilever the first 10 eigenpairs provide 1/50 of the total amount. Thus, it appears to be unnecessary to introduce converged eigenpairs during the updating. This has the benefit of substantially reducing the computational effort.

The following heuristic rule appears to be effective in partly answering question (i): if the higher order RQ energy ratio R_h defined in (17) is less than 10% of the total RQ energy ratio, the eigenpair is classified as member of the low-frequency spectrum, and may be dropped from the parameter update process. A similar rule for separating intermediate and high frequency modes has not yet been established.

7 Concluding remarks

The main objective of this work is to study whether the PVP framework, which provides a systematic way to adjust the stiffness matrix of a static model, can be beneficially extended to problems in structural dynamics.

The first step investigated several techniques for constructing the mass matrix. The definitions of consistent, boundary-consistent and lumped mass matrix have been established for this class of finite elements. Numerical experiments indicate the same frequency convergence rate in the vibrations eigenproblem, suggesting that the simplest (LMM) mass matrix is adequate.

We have shown that the ratio between higher order energy and low order energy, computed for a given mode shape through the Rayleigh Quotient, can be used as an indicator of how well the mesh "captures" that mode. We described how the SB-EBE method can be used as driver for updating the free parameters. In the numerical examples the frequencies show a 5 to 10% improvement. Although this improvement could be considered minor, its effects in the dynamic response are more dramatic, con-

Table 3. SS square plate. Effect of dropping low frequency modes on parameter update

Element number	Parameters computed using modes 1 to 9	Parameters computed using modes 5 to 9
11	2.058	2.040
12	2.058	2.040
13	0.703	0.724
14	2.079	2.047
19	2.058	2.040
20	2.058	2.040
21	1.557	1.550
22	0.703	0.724
23	2.079	2.047

Table 4. Cantilever trapezoidal plate. Effect of dropping low frequency modes on parameter update

Element number	Parameters computed using modes 1 to 20	Parameters computed using modes 10 to 20
7	1.343	1.343
8	1.891	1.889
9	0.858	0.848
10	1.730	1.721
11	1.254	1.255
12	1.765	1.764
13	1.557	1.550
14	1.131	1.136
15	1.628	1.636
16	0.980	0.980
17	1.563	1.563
18	1.332	1.331
19	1.509	1.510
20	1.514	1.514
21	0.995	0.986
22	1.414	1.400
23	1.424	1.439
24	1.653	1.658
25	1.663	1.658
26	1.124	1.162
27	1.258	1.256
28	1.649	1.640
29	1.185	1.185
30	1.525	1.550
31	1.331	1.360
32	1.082	1.057
33	1.497	1.572
34	1.191	1.162
35	1.185	1.163
36	1.740	1.690

Table 5. Values of $\|\mathbf{R}_{1,M}\|_2$ for SS square plate

	with modes 1–9	with modes 5–9
Non updated	456987	441725
Updated	421470	406484

Table 6. Values of $\|\mathbf{R}_{1,M}\|_2$ for cantilever trapezoidal plate

	with modes 1–9	with modes 5–9
Non updated	495203	486671
Updated	475386	467075

sidering the fact that computed *accelerations* are compared. The results presented in Figs. 11 and 15 indicate better phase and amplitude agreement with the refined mesh response.

The SB-EBE updating method is self-contained in the sense that there is no need of feedback information from a finer mesh. This property is important in real-world dynamic models, for which the mesh is constructed once and for all. A note of caution, however, is that the objective function (27) has been so far tested primarily on plate bending problems.

Research is under way to use the free parameters and the SE-EBE technique to detect structural damage in plates. If successful, this approach would represent an important advance in failure localization methodology, which experiences difficulties in passing from skeletal to continuum models.

References

Bergan, P. G.; Hanssen, L. (1976): A new approach for deriving 'good' finite elements. In: Whiteman, J. R. (ed.): Proceedings MAFELAP II Conference, London: Academic Press, 483–498

Bergan, P. G.; Nygård, M. K. (1984): Finite elements with increased freedom in choosing shape functions. Int. J. Num. Meth. Eng. 20, 643–664

Cook, R. D.; Malkus, D. S.; Plesha, M. E. (1989): Concepts and applications of finite element analysis. 3rd ed. Wiley, New York

Farhat, C.; Hemez, F. (1993): Updating finite element dynamic models using an element-by-element sensitivity methodology. A1AA J. 31, 1702–1711

Felippa, C. A. (1994): A survey of parametrized variational principles and applications to computational mechanics. Comp. Meth. Appl. Mech. Eng. 113, 109–139

Felippa, C. A. (1996): Recent developments in parametrized variational principles for mechanics. Comp. Mechanics 18, 159–174

Felippa, C. A.; Bergan, P. (1987): A triangular plate bending element based on an energy orthogonal free formulation. Comp. Meth. Appl. Mech. Eng. 61, 120–160

Felippa, C. A.; Militello, C. (1989) Developments in variational methods for high performance plate and shell elements. In: Analytical and Computational Models for Shells, CED Vol. 3. Noor, A. K.; Belytschko, T.; Simo J. C. (eds.): The American Society of Mechanical Engineers. New York: AME, 191–216

Felippa, C. A.; Militello, C. (1990): Variational formulation of high performance finite elements: parametrized variational principles. Comput. Struct. 36, 1–11

Hemez, F. M. (1993): Theoretical and experimental correlation between finite element models and modal tests in the context of large flexible space structures. Ph. D. Dissertation, Department of Aerospace Engineering Sciences, University of Colorado, Boulder, CO, USA

Militello, C. (1991): Application of parametrized variational principles to the finite element method. Ph. D. Dissertation, Department of Aerospace Engineering Sciences, University of Colorado, Boulder, CO, USA

Militello, C.; Felippa, C. A. (1991a): The Individual Element Test Revisited, In: The Finite Element Method in the 1990s, Ed. by E. Oñate, J. Periaux and A. Samuelsson. Springer-Verlag, Berlin 554–564

Militello, C.; Felippa, C. A. (1991b): The first ANDES elements: 9 d.o.f. plate bending triangles. Comp. Meth. Appl. Mech. Eng. 93, 217–246

Park, K. C.; Stanley, G. M. (1986): A curved C^0 shell element based on assumed natural-coordinate strains. J. Appl. Mech. 53, 278–290

Taylor, R. L.; Simo, J. C.; Zienkiewicz, O. C.; Chan, A. C. H. (1986): The Patch Test – A condition for assessing FEM convergence. Int. J. Num. Meth. Eng. 22, 39–62